Synthesis of magnetic biochar derived from cotton stalks for the removal of Cr(VI) from aqueous solution

Fengfeng Ma, Baowei Zhao and Jingru Diao

ABSTRACT

A magnetic cotton stalk biochar (MCSBC) was synthesized through chemical co-precipitation, based on cotton stalk biochar (CSBC). The MCSBC and CSBC were characterized by scanning electron microscopy, Fourier transform infrared spectroscopy, X-ray diffraction, X-ray photoelectron spectroscopy and vibrating sample magnetometry. The characterization analyses showed that the magnetization process endowed the CSBC with excellent magnetic properties with a superparamagnetic magnetization of 27.59 emu/g. Batch adsorption experiment results indicated that the Cr(VI) maximum adsorption capacity of MCSBC was 20.05 mg/g, which was higher than that of CSBC (18.77 mg/g). The adsorption kinetic data were well fitted by the pseudo-second-order model and the adsorption isotherms were well represented by the Sips isotherm model. The thermodynamic studies indicated that the adsorption process was spontaneous and endothermic, and the entropy increased. The potential adsorption mechanism was the electrostatic adsorption of anionic Cr(VI) to the positively charged MCSBC surface, the reduction of Cr(VI) into Cr(III) and the complexation of Cr(III) by oxygen-containing functional groups of MCSBC. The regeneration studies showed that MCSBC kept 80% of its initial Cr(VI) adsorption capacity in the cycle. All the findings suggest that this novel magnetic biochar could be used in the field of Cr(VI)-containing wastewater treatment.

Key words | adsorption, Cr(VI), magnetic biochar, regeneration

Fengfeng Ma
Baowei Zhao (corresponding author)
Jingru Diao
School of Environmental and Municipal Engineering,
Lanzhou Jiaotong University,
Lanzhou 730070, Gansu,
China
E-mail: *zhbw2001@sina.com*; *baowei.zhao@yahoo.com*; *baoweizhao@mail.lzjtu.cn*

INTRODUCTION

Heavy metals pose a significant risk to the environment and public health due to their toxic properties and potential carcinogenicity. Hexavalent chromium (Cr(VI)) is a common contaminant in water that is mainly emitted from industrial processes such as chromium mining and smelting, metal processing, dyeing, chromium salt manufacturing, electroplating, and leathering (Zhang *et al.* 2018). Cr(VI) is a carcinogenic, mutagenic and teratogenic pollutant that poses serious risks to living organisms and human health. Cr(VI) is a common pollutant in some rural areas in China. For instance, the concentration of Cr(VI) is higher than the allowable limit of 0.05 mg/L in the water of Huan County, Gansu Province (Duan *et al.* 2017).

Currently, several treatment technologies have been developed to remove Cr(VI) ions from the wastewater, including membrane separation, ion exchange, chemical precipitation, and adsorption. Among these technologies, adsorption is one of the most promising methods due to its high efficiency, low cost and easy operation (Mohan *et al.* 2014). The key to the application of adsorption technology in wastewater treatment is the selection of adsorbents. In the past few decades, various types of adsorbents have been widely applied to wastewater treatment (Hsu *et al.* 2009). There have been many studies recently on the production and optimization of adsorbents with high adsorption efficiency and less environmental impact. Biochar is a carbon-rich product obtained by the pyrolysis of biomass under oxygen-free or anoxic conditions (Dong *et al.* 2011). The surface of the biochar is rich in oxygen-containing functional groups, which typically have a net negative charge due to the dissociation of oxygen-containing functional groups (Chen *et al.* 2015). Thus, biochar has been widely used for heavy metals and the removal of organic pollutants from water (Mohan *et al.* 2014). Biochar is generally prepared in the form of a powder, which makes it difficult to separate from water, resulting in filter

doi: 10.2166/wst.2019.208

clogging and secondary contamination (Essandoh *et al.* 2017). The introduction of a magnetic material into the biochar can achieve rapid separation and recovery of the biochar. The effective separation of magnetic biochar from water obviously shortens the duration of the whole decontamination process, accordingly reducing the costs, which is extremely significant in industrial scale application. Additionally, magnetic biochar can be effectively separated and recovered by an external magnetic field, thereby simplifying the treatment process and reducing the energy consumption in the separation process. To endow biochar with a magnetic property and enhance its adsorption capacity for pollutant removal is a potential solution to its disadvantages (Son *et al.* 2018). For example, several studies revealed that Fe_3O_4-based biochars created via chemical co-precipitation are highly effective for the removal of Pb(II) (Karunanayake *et al.* 2018), Cd(II), Cu(II) (Son *et al.* 2018), As (III), and Cr(VI) (Shi *et al.* 2018). At the same time, these results also indicate that the Fe_3O_4-based biochars can be easily separated from water by an external magnetic field. However, few studies have been performed with regard to the preparation of Fe_3O_4-based biochar using cotton stalk as feedstock for the adsorption of Cr(VI) from an aqueous solution, and there is still missing information on the mechanisms of Cr(VI) adsorption after the magnetization process.

Cotton stalk is the main agricultural byproduct in the Chinese countryside, with annual cotton stalk production exceeding 40 million tons (Du *et al.* 2013). Although a small portion of cotton stalk is used as feed, the majority of cotton stalk is incinerated or discarded, causing environmental problems such as air pollution. The utilization of cotton stalk would not only provide an added value to cotton but also help solve agricultural byproduct disposal problems with a positive impact in local and national economies. Thus, in the present study, magnetic biochar was prepared from cotton stalk and used for Cr(VI) removal using the batch adsorption method. The magnetic cotton stalk biochar (MCSBC) was explored through a variety of characterization tools, including vibrating sample magnetometry (VSM), scanning electron microscopy (SEM), Fourier transform infrared (FTIR) spectroscopy, X-ray diffraction (XRD), and X-ray photoelectron spectroscopy (XPS). A batch of adsorption experiments were conducted to determine and compare the properties and adsorption capacity of Cr(VI) onto cotton stalk biochar (CSBC) and MCSBC. Additionally, the adsorption mechanisms and the recycling and regeneration performance of the MCSBC were investigated.

MATERIALS AND METHODS

Preparation of CSBC and MCSBC

Cotton (*Gossypium* spp. L.) stalk was collected from farmland in Korla, Xinjiang Uygur Autonomous Region, China. The detailed preparation method for CSBS was described by Ma *et al.* (2016). The conditions for magnetic CSBC preparation were referenced in Wang *et al.* (2014), and 20 g of dried CSBC was first soaked in a beaker containing 200 mL of deionized water. Then, 20 g $FeCl_3{\cdot}6H_2O$ and 11.1 g $FeSO_4{\cdot}7H_2O$ were dissolved in 600 mL of highly purified water and stirred until they were dissolved completely. Then, two solutions were mixed and stirred at room temperature for 30 min. The pH value of the mixed suspension was adjusted to 11.0 with NaOH solution (10 M), followed by vigorous stirring at 25 °C for 1 h. The suspension was boiled for 1 h and filtered. Then, the filtrate was rinsed several times with deionized water and ethanol and dried at 70 °C for 24 h. The final filtered material was denoted as MCSBC.

Characterization of CSBC and MCSBC

The element content (C, H, and N) of CSBC and MCSBC was determined by using an element analyzer (Heraeus, Germany). The surface areas of CSBC and MCSBC were quantified based on N_2 multilayer adsorption using a surface area analyzer (Micromeritics ASAP 2010, USA) and calculated according to the multipoint Brunauer–Emmett–Teller (BET) method. The morphology of MCSBC was studied using SEM (JSM-5600 LV, Japan). The magnetic properties of MCSBC were assessed using a vibrating sample magnetometer (EZ-9, USA). FTIR spectroscopy (Nexus870, USA) was used to analyze the functional groups of the MCSBC and post-adsorption MCSBC. The crystallographic structures of the MCSBC and post-adsorption MCSBC were obtained by XRD analysis, using an X'Celerator diffractometer (PAN-alytical, Holland) with a Cu Kα radiation. XPS spectra of the samples were obtained using an ESCALAB 250 Xi (Thermo Fisher Scientific, USA) with a monochromated Al Kα X-ray radiation source and a hemispherical electron analyzer.

Batch adsorption experiments

The stock solution of Cr(VI) (1,000 mg/L) was prepared by dissolving analytical grade potassium dichromate ($K_2Cr_2O_7$) into deionized water. For the kinetics experiments, 0.10 g adsorbent (CSBC or MCSBC) was added into conical vitreous vessels with a 20 mL solution of $K_2Cr_2O_7$ (pH = 3.0 ± 0.1,

100 mg/L). The closed vessels were placed on a shaker (CHA-S Shaker, Jintan Danyang Instrumental Company, China) at 150 rpm under 25 °C. At appropriate intervals (0.17–24 h), the mixtures were immediately filtered through a 0.45 μm nylon membrane. The adsorption isotherms for Cr(VI) on the adsorbent (CSBC or MCSBC) were determined using 0.10 g biochar with 20 mL Cr(VI) solutions, and Cr(VI) concentrations of 10–500 mg/L in a batch of conical vessels. The vessels were agitated on a shaker for 24 h under 25 °C. Then the mixtures were separated by filtration to determine the Cr(VI) concentration in the filtrate.

To investigate the effect of the pH value of solution on the Cr(VI) adsorption onto MCSBC, 0.10 g of MCSBC was added into a 20 mL Cr(VI) solution (100 mg/L) with the pH value of the solution varying from 2.0 to 10.0. The initial pH value of the solution was adjusted using NaOH (0.1 M) or HCl (0.1 M). The Cr(VI) concentration was analyzed with the diphenyl hydrazine spectrophotometry method via a UV-vis spectrophotometer (UV-1800, Shanghai) at 540 nm.

Regeneration performance

The MCSBC was introduced into the Cr(VI) solution (pH = 3.0 ± 0.1, 100 mg/L) with an MCSBC dosage of 15 g/L, and then shaken at 25 °C for 24 h. After filtration, the Cr(VI) concentration in the filtrate was analyzed to determine the amount of adsorbed Cr(VI) on the MCSBC. Then, the MCSBC after adsorption of Cr(VI) was collected and a 0.1 M NaOH solution was used to desorb Cr(VI) from the MCSBC. The regenerated MCSBC was used in the next adsorption–desorption cycle for Cr(VI). Six adsorption-desorption cycles were performed in this study.

Adsorption models

Kinetic studies of the Cr(VI) adsorption onto CSBC and MCSBC were carried out using the following adsorption models. The pseudo-first-order model (Equation (1)), pseudo-second-order model (Equation (2)), Elovich (Equation (3)), and intra-particle diffusion model (Equation (4)) can be expressed as:

$$\frac{\mathrm{d}q_t}{d_t} = k_1 (q_e - q_t) \tag{1}$$

$$\frac{dq_t}{d_t} = k_2 (q_e - q_t)^2 \tag{2}$$

$$\frac{dq_t}{d_t} = \alpha \exp(-\beta q_t) \tag{3}$$

$$q_t = k_d^{1/2} + C_i \tag{4}$$

where q_t (mg/g) and q_e (mg/g) are the amount of Cr(VI) adsorbed at time t (h) and at equilibrium, respectively; k_1 (h^{-1}), k_2 (g/mg·h), and k_d (mg/g·$h^{-1/2}$) are the pseudo-first-order, pseudo-second-order, and intra-particle diffusion rate constants, respectively; α (mg/g·h) is the initial adsorption rate, β (g/mg) is the desorption constant, and C_i is a constant that relates to the boundary layer thickness.

Four adsorption isotherm models, Langmuir (Equation (5)), Freundlich (Equation (6)), Sips (Equation (7)), and Temkin (Equation (8)), were used to fit the isotherm data.

$$q_e = \frac{q_m K_L c_e}{1 + K_L c_e} \tag{5}$$

$$q_e = K_F c_e^{1/n} \tag{6}$$

$$q_e = \frac{q_m K_S c_e^{\frac{1}{n}}}{1 + K_S c_e^{\frac{1}{n}}} \tag{7}$$

$$q_e = A \ln K_t c_e \tag{8}$$

where q_e is the equilibrium adsorption amount of Cr(VI) (mg/g), q_m is the theoretical saturation capacity (mg/g), c_e is the equilibrium concentration of Cr(VI) in the aqueous solution (mg/L), and K_L is the Langmuir constant (L/mg); K_F (L/mg) and n (dimensionless) are the Freundlich isotherm constants; K_S is the Sips model constant; A and K_t are the constants of the Temkin isotherm model.

RESULTS AND DISCUSSION

Characterizations of CSBC and MCSBC

The physical and chemical properties of CSBC and MCSBC are presented in Table 1. The yield of the CSBC was 34.51%. The carbon content of CSBC was lower than that of MCSBC, and very little H and N were observed in CSBC and MCSBC. The nitrogen adsorption analysis results of

Table 1 | Physical characteristics and elemental composition of CSBC and MCSBC

	CSBC	MCSBC
Yield (%)	34.51	/
C (%)	48.65	53.69
H (%)	4.21	2.26
N (%)	3.43	0.95
pH_{pzc}	4.08	5.13
Surface area (m^2/g)	29	42
Pore volume (cm^3/g)	0.027	0.076

CSBC and MCSBC are also given in Table 1. Compared with CSBC, for MCSBC, the specific surface area increased from 29 m^2/g to 42 m^2/g, and the total pore volume increased from 0.027 cm^3/g to 0.076 cm^3/g.

The values of the point of zero charge (pH_{pzc}) of CSBC and MCSBC are presented in Table 1. The pH_{pzc} of MCSBC (5.13) is higher than that of CSBC (4.08). This phenomenon of increased pH_{pzc} may be caused by the introduction of Lewis basic groups (i.e., –OH) after Fe_3O_4 particles were attached on the surface of the CSBC (Zhang *et al.* 2018). A high value of pH_{pzc} is more favorable for Cr(VI) adsorption, which is often present under acidic conditions (Shi *et al.* 2018).

The morphology and structures of CSBC and MCSBC are compared by SEM graphs (Figure S1, available with the online version of this paper). The SEM graph of the CSBC shows a relatively plain and smooth surface (Figure S1(a)). However, the surface of the MCSBC was more porous and coarser than that of the CSBC, and there are many irregular iron oxide particles in the MCSBC (Figure S1(b)). The irregular iron oxide particles that dispersed on the MCSBC surface helped to keep the rugged morphological structure of MCSBC. These irregular iron oxide particles were probably Fe_3O_4 particles (Figure 1(b)). This result indicates that Fe_3O_4 has been loaded onto the surface of the CSBC. These surface structure changes increase the specific surface area of the CSBC (Table 1), which may provide more Cr(VI) adsorption sites.

The FTIR spectra and spectroscopic assignment of CSBC, MCSBC and MCSBC after Cr(VI) adsorption are shown in Figure 1(a). As shown in Figure 1(a), the FTIR spectra of CSBC and MCSBC show several characteristic peaks appearing in the wavenumber range of 400–4,000 cm^{-1}. The peak at 3,417 cm^{-1} belonged to the stretching vibration of the hydroxyl groups (Mia *et al.* 2017). The peaks at 2,921 cm^{-1} and 2,846 cm^{-1} were assigned to the $–CH_2$ and $–CH_3$ groups, respectively. The aromatic C=C stretching and C=O stretching of the conjugated ketones and quinines were determined to be peaks at 1,589 cm^{-1} and 1,700 cm^{-1}, respectively (Mia *et al.* 2017). The peak at 1,380 cm^{-1} was caused by the $–CH_2–$ bond deformation vibrations. The peak at 1,124 cm^{-1} was assigned to the C-O stretching vibration group. These results indicate that various oxygen-containing functional groups were present on the CSBC and MCSBC. A difference in the FTIR spectra between the CSBC and MCSBC was the new peak at 578 cm^{-1} that appeared in the MCSBC, which represented Fe-O (Zhou *et al.* 2017).

The XRD patterns of CSBC and MCSBC are shown in Figure 1(b). The diffraction spectrum of CSBC did not show any significant crystallization peaks, indicating the amorphous phase of the CSBC. However, the XRD showed that the structure and purity of the crystallization MCSBC peaks were keen-edged at $2\theta = 30.31°$, 35.71°, 37.34°, 43.41°, 57.46°, and 62.91°, showing limited noise, and were consistent with the phase of Fe_3O_4 (Guo *et al.* 2015). No other sharp peaks were found, confirming that magnetite is the main crystallites phase in MCSBC. The findings demonstrate that the magnetic iron-coated CSBC was successfully synthesized.

XPS is used to analyze the chemical compositions and chemical status of an element. The XPS spectra of the CSBC and MCSBC are shown in Figure 2. As shown in Figure 2(a), the CSBC surface was rich in only carbon and oxygen, while Fe and Cr appeared on MCSBC and MCSBC after adsorption of Cr(VI), respectively. The chrome content increased significantly and the oxygen

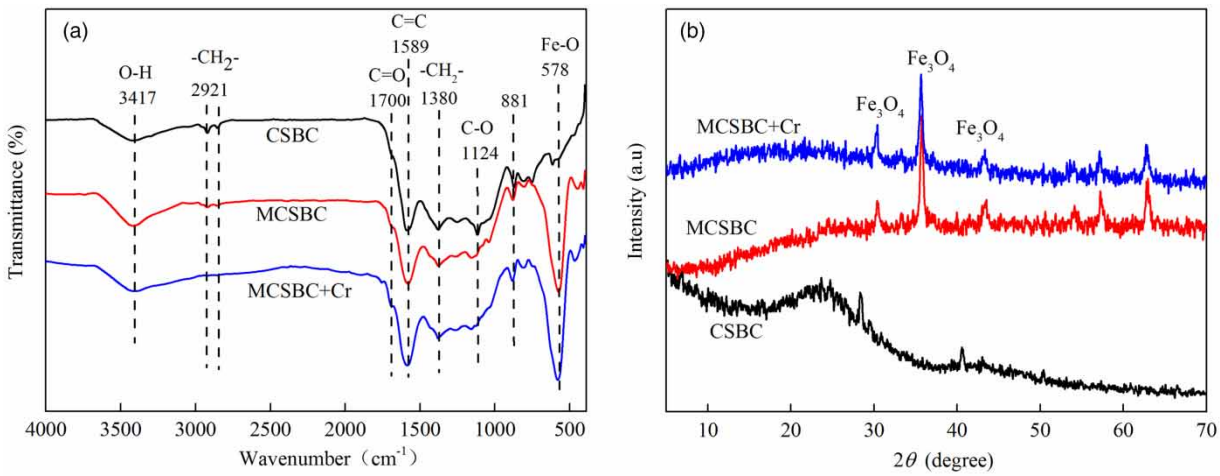

Figure 1 | FTIR spectrum (a) and XRD pattern (b) of CSBC, MCSBC, and MCSBC with Cr(VI) adsorption.

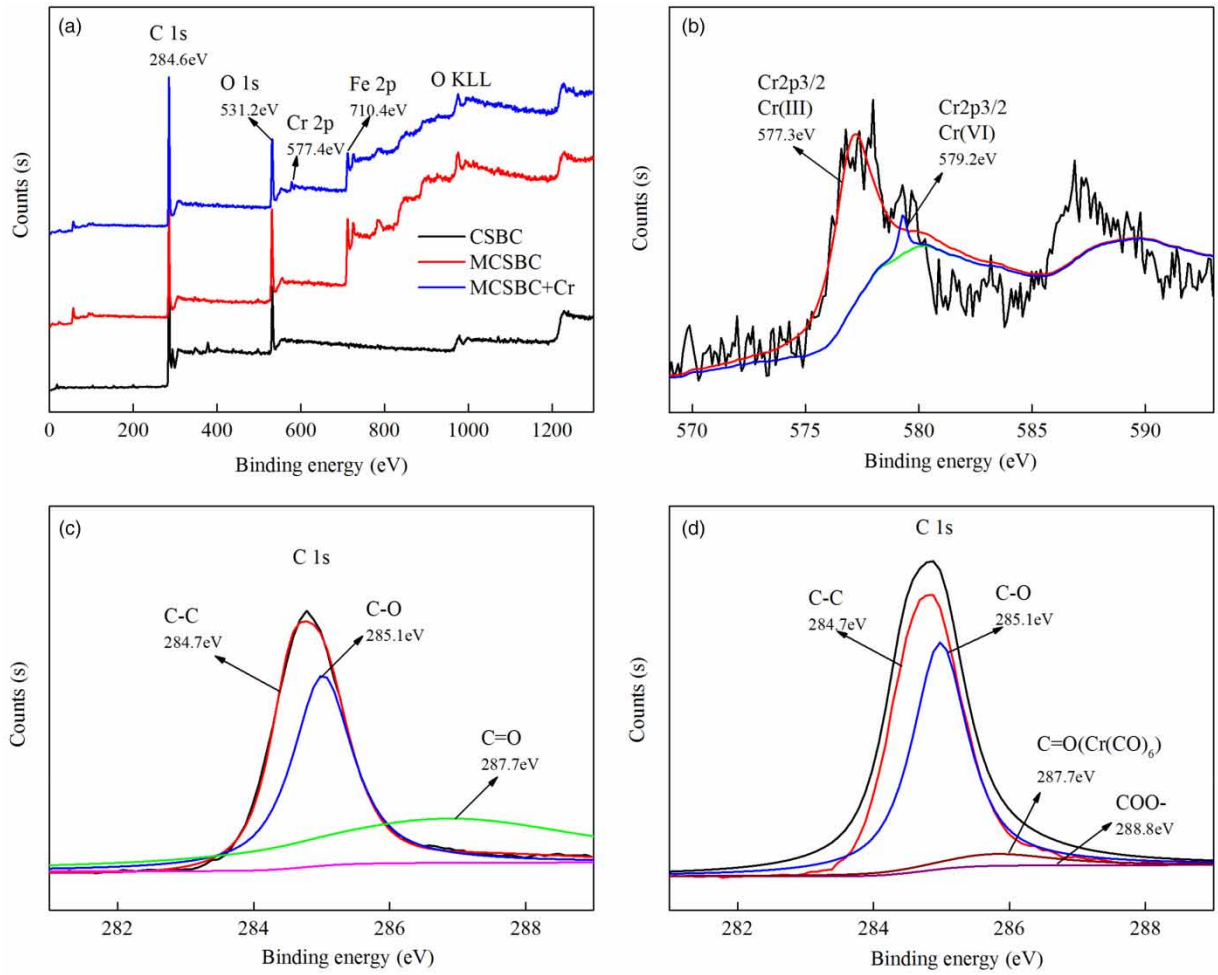

Figure 2 | (a) XPS spectrum of CSBC, MCSBC, and MCSBC with Cr(VI) adsorption; (b) deconvolution of Cr 2p of MCSBC with Cr(VI) adsorption; (c) C 1s of MCSBC; (d) C 1s of MCSBC with Cr(VI) adsorption.

content decreased, indicating that the oxygen-containing functional groups may participate in the adsorption of Cr(VI). The C 1s XPS spectra of MCSBC shown in Figure 2(c) could be fitted to three peaks at 284.7 eV, 285.1 eV, and 287.7 eV. The main peak at 284.7 eV was caused by the sp^2 hybridized orbital that could be ascribed to a C–C bond (Zhu *et al.* 2017). The main peaks at 285.1 eV and 287.7 eV were assigned to C–O and C=O groups, respectively (Zhu *et al.* 2017). As shown in Figure 2(d), the C 1s XPS spectra of MCSBC after adsorption of Cr(VI) indicated that the four components corresponded to C–C (284.7 eV), C–O (285.1 eV), C=O ($Cr(CO_6)$) (287.7 eV), and COO– (288.8 eV). These results indicated that MSCBC had a considerable amount of oxygen-containing functional groups on its surface, which is beneficial for the adsorption Cr(VI) ions by MCSBC.

The magnetic property of MCSBC was measured by VSM at room temperature. The magnetic hysteresis curve of MCSBC is presented in Figure 3. The results showed that the saturation magnetization of MCSBC was 27.59 emu/g, which was lower than that of pure Fe_3O_4 materials (58.94 emu/g) (Wang *et al.* 2014). This discrepancy may be due to the smaller size of the magnetite combination on the MCSBC. In addition, the inset picture indicates that the MCSBC could be easily separated from the solution by a permanent magnet. These results confirmed that the MCSBC was magnetic and can be used as a magnetic adsorbent to remove heavy metals in the liquid phase.

Adsorption kinetics

The kinetics of Cr(VI) adsorption was investigated to understand the potential rate-controlling step and mechanism of Cr(VI) adsorption. Figure 4(a) shows the effect of the contact time on Cr(VI) adsorption by the CSBC and MCSBC. It can be seen that the Cr(VI) adsorption capacity at time t

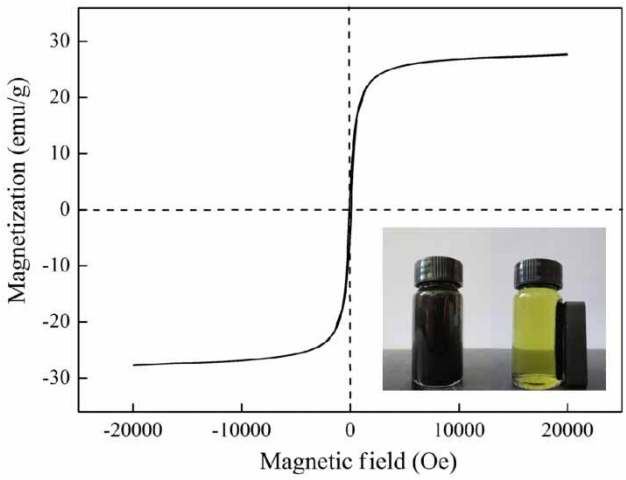

Figure 3 | Magnetic hysteresis curve of the MCSBC.

(q_t) is almost unchanged after 4 h for both the CSBC and MCSBC. Therefore, 4 h can be considered as the optimal adsorption time for the adsorption process to reach equilibrium. When comparing the adsorption capacity, MCSBC showed a higher Cr(VI) adsorption capacity than CSBC. In this study, Fe_3O_4 particles on the MCSBC could increase the BET surface area (Table 1) as well as the functional groups of MCSBC, which facilitate the Cr(VI) adsorption.

Based on the experimental data, the adsorption kinetics of Cr(VI) on CSBC and MCSBC (Figure 4(a)) was fitted using Elovich, pseudo-first- and pseudo-second-order models. The best-fit parameters of these models are listed in Table 2. It can be concluded from Table 2 that the magnitude of the coefficient of determination (R^2) follows the order of pseudo-second-order > Elovich > pseudo-first-order. Moreover, the q_e value predicted from the pseudo-second-order model as well as maximal adsorption capacity (q_m, Table 2) of the CSBC and MCSBC were close to the experimental q_e value. This result illustrated that the pseudo-second-order model was the preferred kinetic adsorption model for Cr(VI) on the CSBC and MCSBC, which was also reported for another magnetic biochar (Zhang *et al.* 2018). The results indicated that the chemical adsorption was the rate-limiting step of the Cr(VI) adsorption onto the CSBC and MCSBC (Venkateswarlu *et al.* 2016). Moreover, the k_2 values and adsorption capacity (q_m, Table 2) of MCSBC were higher than those of the CSBC, indicating that the MCSBC has a higher Cr(VI) capacity and the magnetization could enhance Cr(VI) adsorption.

To further understand the rate-controlling steps and the adsorption mechanism, the intra-particle diffusion model was used to fit the adsorption kinetic data. By plotting q_t versus $t^{1/2}$ of Equation (4), the steps of the Cr(VI) adsorption onto the CSBC and MCSBC can be described in detail and the corresponding rate constants are estimated by a linear regression. The linear regressions of the intra-particle diffusion model of the Cr(VI) adsorption onto the CSBC and MCSBC are shown in Figure 4(b). As seen from Figure 4(b) and Table 2, the two stages are detailed well following the rate constants order of $k_{d1} > k_{d2}$, which indicated a rate decrease occurred in Cr(VI) adsorption onto the CSBC and MCSBC. The first stage represented the diffusion of Cr(VI) through the solution to the surface of the CSBC or MCSBC and the instantaneous adsorption with the highest rate constants. The second stage was attributed to intra-particle diffusion with a lower rate constant (Albadarin *et al.* 2012). In particular, the rate constant of the second

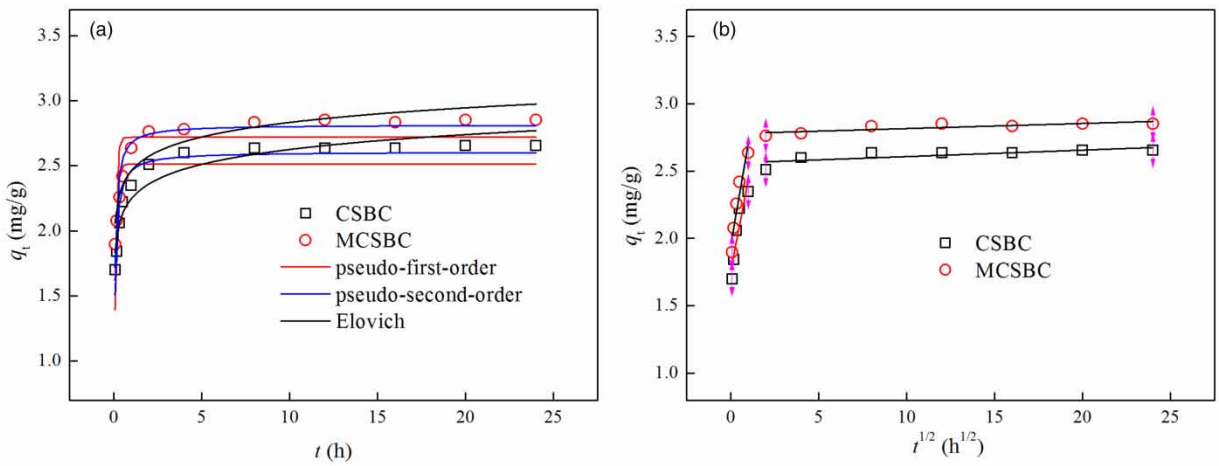

Figure 4 | (a) Fitting of Elovich, pseudo-first- and pseudo-second-order models for adsorption of Cr(VI) on CSBC and MCSBC. (b) Intra-particle diffusion plots for adsorption of Cr(VI) on CSBC and MCSBC.

Table 2 | Kinetic parameters of Cr(VI) adsorption on CSBC and MCSBC

	Pseudo-first-order			Pseudo-second-order			Elovich		
Adsorbents	q_m (mg/g)	k_1 (h^{-1})	R^2	q_m (mg/g)	k_2 (g/mg/h)	R^2	α (mg/g·h)	β (g/mg)	R^2
CSBC	2.51	9.72	0.623	2.61	6.32	0.916	2.24	6.06	0.902
MCSBC	2.72	10.87	0.619	2.81	6.72	0.922	2.46	6.19	0.873
	Intra-particle diffusion								
Adsorbents	k_{d1}	C_1	R^2	k_{d2}	C_2	R^2			
CSBC	0.67	1.75	0.798	0.0048	2.56	0.523			
MCSBC	0.76	1.94	0.881	0.0038	2.78	0.639			

stage (k_{d2}) was much lower than that of the first stage ($k_{d1} > k_{d2}$), while C_1 is less than C_2, which indicates that the rate of Cr(VI) adsorption was higher in the beginning of adsorption due to large available surface area of the CSBC and MCSBC. On the other hand, the adsorption of Cr(VI) by the MCSBC is superior to that of the CSBC, evidenced by the higher rate constant of first stage. Furthermore, none of the plots pass through the origin (Figure 4(b)), suggesting that the intra-particle diffusion was part of the adsorption process, but it was not the only rate-controlling step. Some other mechanisms, such as ion exchange or complexes, can also control the rate of adsorption (Zhou *et al.* 2016).

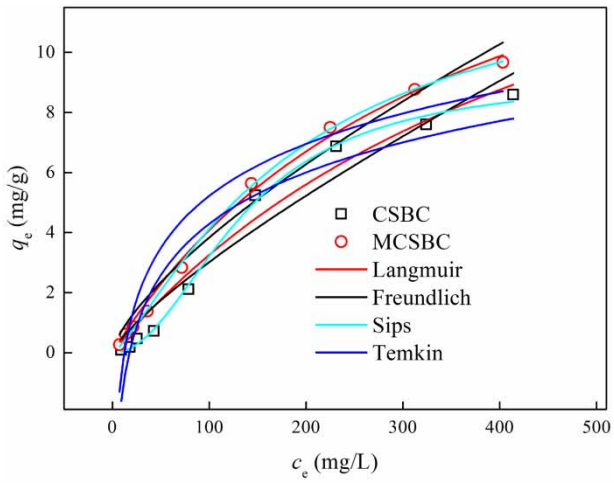

Figure 5 | Adsorption isotherms of Cr(VI) on CSBC and MCSBC.

Adsorption isotherms

The adsorption isotherms of Cr(VI) adsorption onto CSBC and MCSBC are presented in Figure 5. The fitting parameters from the isotherm models are listed in Table 3. From Table 3, the Sips model was better at explaining the mechanism of Cr(VI) adsorption by the CSBC and MCSBC, having the highest coefficient of determination ($R^2 = 0.997$, 0.999) values. The Sips model is a combined form of Langmuir and Freundlich isotherm models and used to predict the heterogeneous adsorption systems. The Sips model is the best-fit isotherm and confirms the heterogeneity of the adsorption process for Cr(VI) adsorption onto MCSBC. This result means that adsorption was diffusion-controlled at low Cr(VI) concentrations, and monomolecular adsorption with saturated values occurred at high Cr(VI) concentrations (Hokkanen *et al.* 2015). The Cr(VI) adsorption capacities of CSBC and MCSBC were 9.17 and 13.26 mg/g respectively. This result may be because MCSBC has a higher surface area, which provides more adsorption sites for Cr(VI).

Table 3 | Isotherm parameters of Cr(VI) adsorption on CSBC and MCSBC

	Langmuir			Freundlich			Sips				Temkin		
Adsorbents	q_m	K_L	R^2	K_F	n	R^2	q_m	K_S	n	R^2	A	K_t	R^2
CSBC	20.05	0.0019	0.969	0.078	1.26	0.949	9.17	0.017	0.48	0.997	2.47	0.057	0.897
MCSBC	18.77	0.0028	0.995	0.144	1.41	0.979	13.26	0.019	0.77	0.999	2.51	0.081	0.913

Table 4 | Thermodynamic parameters of Cr(VI) adsorption on CSBC and MCSBC

Adsorbents	ΔG^0 (kJ/mol)			ΔH^0 (kJ/mol)	ΔS^0 (J/mol·K)
	298 K	308 K	318 K		
CSBC	−4.36	−5.95	−6.04	63.34	254.17
MCSBC	−6.06	−6.53	−7.09	23.14	128.57

Adsorption thermodynamics

Thermodynamic theory assumes that the entropy change is the driving force behind energy inaccessibility and loss in isolated systems (Lei *et al.* 2017). The Gibbs free energy change (ΔG^0) is related to the standard enthalpy change (ΔH^0) and standard entropy change (ΔS^0). The thermodynamic parameters for Cr(VI) adsorption by CSBC and MCSBC are listed in Table 4. As the temperature increases, the value of ΔG^0 becomes more negative, indicating that the adsorption of Cr(VI) on CSBC and MCSBC is more favorable and the adsorption process was spontaneous in nature. The positive values of ΔH^0 proved that the Cr(VI) adsorption on CSBC and MCSBC was an endothermic process. The values of ΔS^0 were also positive, which indicated that there was an increase of randomness at the solid/solution interface during adsorption of Cr(VI) on CSBC and MCSBC. All the thermodynamic parameters may also suggest that the elevated temperature provides sufficient energy for the Cr(VI) ions to overcome the diffusion layer and be adsorbed onto the interface structure of the CSBC and MCSBC.

Effect of pH value of solution

The effect of the initial pH value of solution on the Cr(VI) adsorption by MCSBC was investigated. Figure 6 shows that the Cr(VI) adsorption capacity was quite dependent on the pH value of the solution: the increase in the pH value of solution reduced the Cr(VI) adsorption capacity. The highest Cr(VI) adsorption capacity was found at pH = 2.0. As the pH value of the solution increased, the adsorption capacity of Cr(VI) decreased sharply. The higher adsorption capacities at lower pH values of the solution (pH = 2 and 3) were similar and demonstrated that the Cr(VI) adsorption by the MCSBC was suitable for acidic conditions. The degree of iron leaching in the aqueous solution at different pH values was investigated using ICP-OES (inductively coupled plasma optical emission spectrometry) after Cr(VI) adsorption. The results showed that there was less than 0.1 mg/L of iron dissolved in the aqueous solution after adsorption, indicating that the pH value of solution has little effect on the Fe oxides deposited on the surface of the MCSBC. The species distribution of Cr(VI) and the surface properties of MCSBC were possible explanations that accounted for this phenomenon. In one sense, the charge of the MCSBC is dependent on the pH value of the solution, by protonation and deprotonation. When the pH value of the solution is less than pH_{pzc} (5.13), anionic Cr(VI) is adsorbed onto the MCSBC by attracting the positively charged surface of MCSBC ($-OH_2^+$). When the pH value of the solution is less than pH_{pzc}, some Cr(VI) can replace the –OH on the MCSBC, but the adsorption capacity of Cr(VI) is significantly reduced. As the pH value of the solution continuously increases, the OH^- competes with the Cr(VI) more intensely, and the OH^- occupies the adsorption site of the MCSBC surface. In another sense, the species distribution of chromium varies with the pH value of the solution, and $HCrO_4^-$ and $Cr_2O_7^{2-}$ are the main forms present in the solution under acidic conditions (pH < 2.0) (Zhou *et al.* 2016). Thus, at lower pH values of the solution, the chromium anions could easily bind with the positively charged MCSBC through electrostatic attraction. MCSBC contains polycyclic aromatics and oxygen-containing functional groups and the MCSBC can serve as an efficient electron-donor for Cr(VI) ions reduction according to Equations (9) and (10) (Hsu *et al.* 2009; Shi *et al.* 2018).

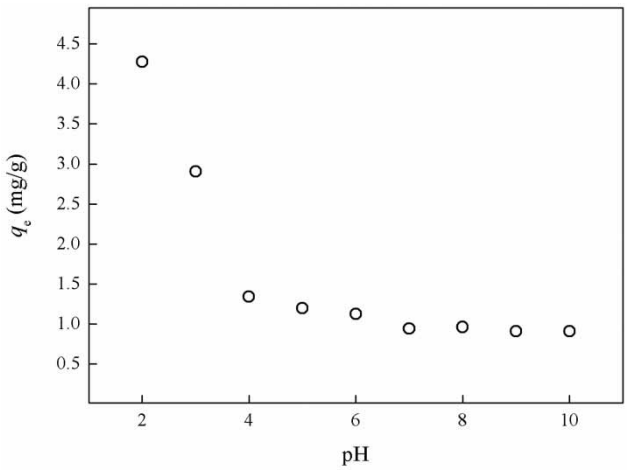

Figure 6 | Effect of the pH value of the solution on Cr(VI) adsorption on MCSBC.

$$HCrO_4^- + 7H^+ + 3e^- \rightarrow Cr^{3+} + 4H_2O \quad (9)$$

$$3C_XOH + Cr_2O_7^{2-} + 4H^+ \rightarrow 3C_XO + Cr^{3+} + 3H_2O \quad (10)$$

There often exists simultaneously various substances in actual wastewater, which may potentially interfere with the Cr(VI) adsorption. The impact of these different factors on the adsorption process deserves further study.

The potential adsorption mechanism

The FTIR spectra of the MCSBC before and after adsorption of Cr(VI) were analyzed to investigate the adsorption mechanism. As shown in Figure 1(a), a change of MCSBC functional groups was observed after Cr(VI) adsorption. The peaks of FTIR at 3,417 cm^{-1} (–OH) and 1,700 cm^{-1} (C=O) decreased after Cr(VI) adsorption. These changes indicated that these groups may be involved in the adsorption of Cr(VI). The above results are in good agreement with other studies (Zhou *et al.* 2016; Zhang *et al.* 2018), which suggested that hydroxyl and carboxylate groups are the primary functional groups for the adsorption of heavy metals.

Furthermore, the XPS analysis of MCSBC before and after Cr(VI) adsorption indicated that Cr(VI) was successfully adsorbed onto the surface of the MCSBC. As shown in Figure 2(a), the C content was increased while the O and Fe contents were decreased after Cr(VI) adsorption. However, there was no significant difference in the C peaks between the MCSBC before and after Cr(VI) adsorption, suggesting that carbon did not contribute to the Cr(VI) adsorption onto MCSBC (Figure 2(c) and 2(d)). For oxygen, oxygen-containing functional groups increase after magnetization and decrease after Cr(VI) adsorption, which indicates that oxygen had a greater adsorption effect on MCSBC adsorption of Cr(VI). A difference in the FTIR spectra between the MCSBC before and after Cr(VI) adsorption onto MCSBC was the new peak at 881 cm^{-1}. According to a previous article (Dong *et al.* 2011), this peak was charged to Cr-O. These changes indicated that the oxygen-containing functional groups were the main reason for effective Cr(VI) adsorption onto MCSBC. In the XPS spectrum of MCSBC after Cr(VI) adsorption (Figure 2(b)), the valences of Cr 2p were separated at 577.3 eV (Cr $2p_{1/2}$) and 579.2 eV (Cr $2p_{3/2}$), which were attributed to Cr(III) and Cr(VI), respectively . These results demonstrated that Cr(VI) in the solution first loaded onto the surface of MCSBC during the adsorption process then reduced to Cr(III) by a heterogeneous redox process (Chen *et al.* 2017).

According to the XRD spectra (Figure 1(b)), the crystal lattice of Fe_3O_4 did not change, and no new crystal shape was formed during the Cr(VI) adsorption onto MCSBC. The result showed that Cr(VI) was adsorbed on the surface of MCSBC through monolayer adsorption, but there was no aggregation or precipitation reaction on the surface of MCSBC.

Based on the above analysis and discussions, we hypothesized that the Cr(VI) adsorption mechanisms of MCSBC could be divided into three processes. First, under strongly acidic conditions, oxygen-containing functional groups such as hydroxyl and carboxyl groups on the MCSBC surface could be easily protonated, and the negatively charged Cr(VI) species were migrated to the positively charged surface of the MCSBC by electrostatic interaction. Second, the adsorbed Cr(VI) anions were reduced to Cr(III) anions by the participation of hydrogen ions and the electron-donor groups were mainly inherited from the MCSBC. Finally, part of the newly formed Cr(III) anions were chelated by the oxygen-containing functional groups of MCSBC.

Reusability of MCSBC

The regeneration and recycling performance of the adsorbent is an important aspect for its practical application. As shown in Figure S2 (available with the online version of this paper), the results of the regeneration experiment indicated that the Cr(VI) adsorption of MCSBC maintains 80% of the initial adsorption capacity at the sixth cycle. The regeneration and recycling studies have confirmed that MCSBC was an easy-to-reuse adsorbent, making it cost effective. The tendency for the decrease in adsorption capacity could be attributed to the loss of the MCSBC dose and the changes in the physical and chemical properties of the MCSBC, such as the reduction in the specific surface area and pore volume and the weakness of the functional groups.

CONCLUSIONS

A facile and inexpensive CSBC was modified with magnetization in a simple and convenient process, and MCSBC was suitable for Cr(VI) removal in an aqueous solution. The magnetization process significantly increased the oxygen-containing functional groups and enhanced the physicochemical properties. Therefore, the adsorption capacity of MCSBC was higher than that of CSBC. The kinetics and isotherms data of Cr(VI) adsorption onto MCSBC were well described with the pseudo-second-order model and Sips isotherm model, respectively. The Cr(VI) adsorption mechanisms include electrostatic interaction of Cr(VI) coupled with Cr(VI) reduction and the complexation of Cr(III), according to the results of FTIR and XPS analyses. In summary, the results obtained from this study indicated that the MCSBC presented a new opportunity to remove Cr(VI) from aqueous solution in an environmentally friendly and efficient manner.

ACKNOWLEDGEMENTS

This study was supported by the National Natural Science Foundation of China (21167007, 21467013, 51766008), the Gansu Province Science and Technology Foundation for youths (18JR3RA129) and Specialized Research Fund for the Doctoral Program of Higher Education of China (20136204110003).

REFERENCES

Albadarin, A. B., Mangwandi, C., Al-Muhtaseb, A. a. H., Walker, G. M., Allen, S. J. & Ahmad, M. N. M. 2012 Kinetic and thermodynamics of chromium ions adsorption onto low-cost dolomite adsorbent. *Chemical Engineering Journal* **179**, 193–202.

Chen, G., Feng, J., Wang, W., Yin, Y. & Liu, H. 2017 Photocatalytic removal of hexavalent chromium by newly designed and highly reductive TiO_2 nanocrystals. *Water Research* **108**, 383–390.

Chen, Z., Xiao, X., Chen, B. & Zhu, L. 2015 Quantification of chemical states, dissociation constants and contents of oxygen-containing groups on the surface of biochars produced at different temperatures. *Environmental Science & Technology* **49** (1), 309–317.

Dong, X., Ma, L. Q. & Li, Y. 2011 Characteristics and mechanisms of hexavalent chromium removal by biochar from sugar beet tailing. *Journal of Hazardous Materials* **190** (1), 909–915.

Du, S.-k., Zhu, X., Wang, H., Zhou, D., Yang, W. & Xu, H. 2013 High pressure assist-alkali pretreatment of cotton stalk and physiochemical characterization of biomass. *Bioresource Technology* **148**, 494–500.

Duan, S., Ma, W., Pan, Y., Meng, F., Yu, S. & Wu, L. 2017 Synthesis of magnetic biochar from iron sludge for the enhancement of Cr(VI) removal from solution. *Journal of the Taiwan Institute of Chemical Engineers* **80**, 835–841.

Essandoh, M., Wolgemuth, D., Pittman, C. U., Mohan, D. & Mlsna, T. 2017 Adsorption of metribuzin from aqueous solution using magnetic and nonmagnetic sustainable low-cost biochar adsorbents. *Environmental Science And Pollution Research* **24** (5), 4577–4590.

Guo, X., Mao, F., Wang, W., Yang, Y. & Bai, Z. 2015 Sulfhydryl-modified Fe_3O_4@SiO_2 core/shell nanocomposite: synthesis and toxicity assessment in vitro. *ACS Applied Materials & Interfaces* **7** (27), 14983–14991.

Hokkanen, S., Repo, E., Lou, S. & Sillanpää, M. 2015 Removal of arsenic(V) by magnetic nanoparticle activated microfibrillated cellulose. *Chemical Engineering Journal* **260**, 886–894.

Hsu, N.-H., Wang, S.-L., Lin, Y.-C., Sheng, G. D. & Lee, J.-F. 2009 Reduction of Cr(VI) by crop-residue-derived black carbon. *Environmental Science & Technology* **43** (23), 8801–8806.

Karunanayake, A. G., Todd, O. A., Crowley, M., Ricchetti, L., Pittman, C. U., Anderson, R., Mohan, D. & Mlsna, T. 2018 Lead and cadmium remediation using magnetized and nonmagnetized biochar from Douglas fir. *Chemical Engineering Journal* **331**, 480–491.

Lei, C., Zhu, X., Zhu, B., Jiang, C., Le, Y. & Yu, J. 2017 Superb adsorption capacity of hierarchical calcined Ni/Mg/Al layered double hydroxides for Congo red and Cr(VI) ions. *Journal of Hazardous Materials* **321**, 801–811.

Ma, F., Zhao, B. & Diao, J. 2016 Adsorption of cadmium by biochar produced from pyrolysis of corn stalk in aqueous solution. *Water Science & Technology* **74** (6), 1335–1345.

Mia, S., Dijkstra, F. A. & Singh, B. 2017 Aging induced changes in biochar's functionality and adsorption behavior for phosphate and ammonium. *Environmental Science & Technology* **51** (15), 8359–8367.

Mohan, D., Sarswat, A., Ok, Y. S. & Pittman, C. U. 2014 Organic and inorganic contaminants removal from water with biochar, a renewable, low cost and sustainable adsorbent – a critical review. *Bioresource Technology* **160**, 191–202.

Shi, S., Yang, J., Liang, S., Li, M., Gan, Q., Xiao, K. & Hu, J. 2018 Enhanced Cr(VI) removal from acidic solutions using biochar modified by Fe_3O_4@SiO_2-NH_2 particles. *Science of The Total Environment* **628–629**, 499–508.

Son, E.-B., Poo, K.-M., Chang, J.-S. & Chae, K.-J. 2018 Heavy metal removal from aqueous solutions using engineered magnetic biochars derived from waste marine macro-algal biomass. *Science of The Total Environment* **615**, 161–168.

Venkateswarlu, S., Lee, D. & Yoon, M. 2016 Bioinspired 2D-carbon flakes and Fe_3O_4 nanoparticles composite for arsenite removal. *ACS Applied Materials & Interfaces* **8** (36), 23876–23885.

Wang, S.-y., Tang, Y.-k., Li, K., Mo, Y.-y., Li, H.-f. & Gu, Z.-q. 2014 Combined performance of biochar sorption and magnetic separation processes for treatment of chromium-contained electroplating wastewater. *Bioresource Technology* **174**, 67–73.

Zhang, X., Lv, L., Qin, Y., Xu, M., Jia, X. & Chen, Z. 2018 Removal of aqueous Cr(VI) by a magnetic biochar derived from *Melia azedarach* wood. *Bioresource Technology* **256**, 1–10.

Zhou, L., Liu, Y., Liu, S., Yin, Y., Zeng, G., Tan, X., Hu, X., Hu, X., Jiang, L., Ding, Y., Liu, S. & Huang, X. 2016 Investigation of the adsorption-reduction mechanisms of hexavalent chromium by ramie biochars of different pyrolytic temperatures. *Bioresource Technology* **218**, 351–359.

Zhou, Z., Liu, Y.-g., Liu, S.-b., Liu, H.-y., Zeng, G.-m., Tan, X.-f., Yang, C.-p., Ding, Y., Yan, Z.-l. & Cai, X.-x. 2017 Sorption performance and mechanisms of arsenic(V) removal by magnetic gelatin-modified biochar. *Chemical Engineering Journal* **314**, 223–231.

Zhu, S., Ho, S.-H., Huang, X., Wang, D., Yang, F., Wang, L., Wang, C., Cao, X. & Ma, F. 2017 Magnetic nanoscale zerovalent iron assisted biochar: interfacial chemical behaviors and heavy metals remediation performance. *ACS Sustainable Chemistry & Engineering* **5** (11), 9673–9682.

First received 29 January 2019; accepted in revised form 9 June 2019. Available online 20 June 2019